

Synergism of primary and secondary interactions in a crystalline hydrogen peroxide complex with tin

Received: 29 January 2024

Accepted: 1 July 2024

Published online: 09 July 2024

Check for updates

Alexander G. Medvedev¹, Pavel A. Egorov¹, Alexey A. Mikhaylov¹, Evgeny S. Belyaev², Gayane A. Kirakosyan^{1,2}, Yulia G. Gorbunova^{1,2}, Oleg A. Filippov³, Natalia V. Belkova³, Elena S. Shubina³, Maria N. Brekhovskikh¹, Anna A. Kirsanova⁴, Maria V. Babak⁴✉, Ovadia Lev⁵✉ & Petr V. Prikhodchenko¹✉

Despite the significance of H₂O₂-metal adducts in catalysis, materials science and biotechnology, the nature of the interactions between H₂O₂ and metal cations remains elusive and debatable. This is primarily due to the extremely weak coordinating ability of H₂O₂, which poses challenges in characterizing and understanding the specific nature of these interactions. Herein, we present an approach to obtain H₂O₂-metal complexes that employs neat H₂O₂ as both solvent and ligand. SnCl₄ effectively binds H₂O₂, forming a SnCl₄(H₂O₂)₂ complex, as confirmed by ¹¹⁹Sn and ¹⁷O NMR spectroscopy. Crystalline adducts, SnCl₄(H₂O₂)₂·H₂O₂·18-crown-6 and 2[SnCl₄(H₂O₂)(H₂O)]·18-crown-6, are isolated and characterized by X-ray diffraction, providing the complete characterization of the hydrogen bonding of H₂O₂ ligands including geometric parameters and energy values. DFT analysis reveals the synergy between a coordinative bond of H₂O₂ with metal cation and its hydrogen bonding with a second coordination sphere. This synergism of primary and secondary interactions might be a key to understanding H₂O₂ reactivity in biological systems.

Hydrogen peroxide, a highly stable reactive oxygen species¹, is widely recognized for its vital contributions to diverse cellular functions including protection against oxidative stress, promotion of cellular differentiation, facilitation of cellular proliferation, and participation in redox signaling pathways²⁻⁴. Furthermore, owing to its oxidative properties, H₂O₂ holds significant importance in a range of industrial applications, including bleaching processes, wastewater treatment and various catalytic processes utilized in industry. While H₂O₂ can be employed in a metal-free processes the effectiveness and selectivity of H₂O₂ as an oxidant can be further enhanced through its kinetic activation by metal complexes^{5,6}. For example, the activation of H₂O₂ by its

coordination to heme enables the efficient utilization of H₂O₂ in various biochemical reactions catalyzed by cytochrome P450 heme-containing enzymes⁷. Despite the fundamental importance of these interactions, their molecular mechanism remains unclear due to the transient and labile nature of H₂O₂-metal adducts.

If we consider complexation as a reaction between Lewis acids and bases, the coordination ability of a ligand may be correlated with its basicity, which can be characterized in terms of its basicity constant (pK_b, which is often substituted by the pK_a of the ligand's corresponding conjugate acid) or proton affinity (PA; that is, the enthalpy of the B + H⁺ → BH⁺ reaction, where B = a base). As the PA of H₂O₂ is

¹Kurnakov Institute of General and Inorganic Chemistry, Russian Academy of Sciences, Moscow, Russian Federation. ²Frumkin Institute of Physical Chemistry and Electrochemistry of the Russian Academy of Sciences, Moscow, Russian Federation. ³Nesmeyanov Institute of Organoelement Compounds, Russian Academy of Sciences, Moscow, Russian Federation. ⁴Drug Discovery Lab, Department of Chemistry, City University of Hong Kong, Kowloon, Hong Kong SAR, China. ⁵Casali Center of Applied Chemistry, Hebrew University of Jerusalem, Jerusalem, Israel. ✉e-mail: mbabak@cityu.edu.hk; ovadia@mail.huji.ac.il; prikhman@gmail.com

4 kcal mol⁻¹ less than that of H₂O⁸, the coordination of H₂O₂ at low concentrations with a metal center is thermodynamically unfavorable in aqueous solutions. Indeed, Williams et al. reported that H₂O₂ complexes are thermodynamically unstable in aqueous solution unless the pH is sufficiently high to deprotonate H₂O₂ and thus favor the formation of hydroperoxo coordination compounds⁹. Subsequently, DiPasquale and Mayer demonstrated that H₂O₂ does not displace a very weakly bound perchlorate ligand from the gallium(III) center of a tetraphenylporphyrin complex¹⁰. Thus, as formulated by Mayer, H₂O₂ typically exhibits poor coordination ability due to its rather low PA, which is attributable to its electron-withdrawing hydroxyl (-OH) group being adjacent to an O atom¹⁰. A few examples of H₂O₂ coordinated with cobalt(II), nickel(II), and copper(II) in non-aqueous solutions were recently reported, supported by nuclear magnetic resonance (NMR) and cyclic voltammetry data^{11,12}. In addition, many aqua complexes have been identified in solution and solid forms, but only one complex of H₂O₂ with a metal cation has been isolated and structurally characterized, namely a complex of H₂O₂ and zinc(II)¹³. However, the isomorphous substitution of H₂O₂ with H₂O (in a 50:50 occupancy ratio) disordered the O atoms and tosyl fragments in this complex, preventing the positions of the H₂O₂ protons being determined objectively. In contrast to transition metals, p-block elements do not catalyze H₂O₂ decomposition. For example, tin compounds are known as H₂O₂ stabilizers as Sn^{IV} forms stable hydroperoxo complexes with high peroxide content¹⁴. However, to the best of our knowledge, the coordination of H₂O₂ with Sn^{IV} has not been reported.

Octahedral coordination is typical for Sn^{IV}, but coordinatively unsaturated tin tetrachloride (SnCl₄) is a strong Lewis acid and thus we hypothesized that it can bind H₂O₂ in the absence of ligands of higher basicity. We confirmed this hypothesis by performing ¹¹⁹Sn and ¹⁷O NMR studies that characterized H₂O₂ coordination by SnCl₄ and H₂O₂ substitution by H₂O, methanol (MeOH), and acetonitrile (MeCN) in the Sn^{IV} coordination sphere. In addition, we performed single-crystal X-ray diffraction (scXRD) analysis of two crystalline adducts of H₂O₂ with 18-crown-6, namely [SnCl₄(H₂O₂)₂·H₂O₂·18-crown-6 (**1**) and 2[SnCl₄(H₂O₂)(H₂O)]·18-crown-6 (**2**), which enabled examination of the intermolecular interactions in these structures. Moreover, we performed density functional theory (DFT) modeling to unveil the synergy between various types of bonds in which H₂O₂ is engaged in **1** and **2** and how this effect stabilizes these complexes.

Results and discussion

As H₂O₂ is less basic than other polar solvents⁸ and it does not form homogeneous solutions with non-coordinating solvents, we used neat H₂O₂ both as a ligand and as a solvent to study its interaction with SnCl₄.

¹¹⁹Sn and ¹⁷O NMR studies

The transformation of the Sn^{IV} coordination sphere upon addition of H₂O₂ proposed in Fig. 1A was studied by ¹¹⁹Sn and ¹⁷O NMR spectroscopy (Fig. 1B, C). The coordinatively unsaturated environment of Sn^{IV} in neat SnCl₄ was revealed by its low-field signal in the ¹¹⁹Sn NMR spectrum ($\delta = -150$ ppm; Fig. 1Ba). The ¹⁷O NMR spectrum of anhydrous H₂O₂ had a single signal at 180 ppm and no signals in the region of H₂O, i.e., at approximately 0 ppm, confirming that it contained less than 0.5 wt.% H₂O (Fig. 1Ca). The addition of 1 wt.% H₂O resulted in the appearance of a signal in the ¹⁷O NMR spectrum at -5 ppm that was 0.8% of the integrated intensity of the H₂O₂ signal in this spectrum (Fig. 1Cb).

Careful addition of up to a fourfold molar excess of anhydrous H₂O₂ to SnCl₄ yielded a biphasic mixture (Supplementary Movie 1), whereas addition of a fivefold molar excess of anhydrous H₂O₂ (1:1 v/v) to SnCl₄ yielded a homogeneous mixture. ¹¹⁹Sn NMR spectroscopy of this SnCl₄-5H₂O₂ system revealed a new high-field signal ($\delta_{\text{Sn}} = -554.7$ ppm) assigned to a SnCl₄(H₂O₂)₂ complex **1** (Fig. 1A, 1Bb) and a low-

intensity (3%) signal representing residual SnCl₄. The latter signal was absent in the ¹¹⁹Sn NMR spectra of mixtures containing higher H₂O₂ concentrations (Fig. 1Bc). An H₂O₂ ligand in complex with tin contains two non-equivalent neighboring O atoms and thus its ¹⁷O NMR signals are quadrupole broadened and therefore not detectable. As such, only one signal was present in the ¹⁷O NMR spectrum ($\delta_{\text{O}} = 185.3$ ppm) and was assigned to free H₂O₂ (Fig. 1Cc). In the ¹¹⁹Sn NMR spectra, a previously small signal at approximately -562 ppm became larger as the H₂O₂-to-SnCl₄ ratio increased (to 9:1; Fig. 1Bc) and was assigned to the complex bearing a bridging aqua ligand [SnCl₄(H₂O₂)₂(μ -H₂O) (**1'**; Fig. 1A). Addition of H₂O to give a 0.5 H₂O-to-SnCl₄ molar ratio resulted in [SnCl₄(H₂O₂)₂(μ -H₂O) being the dominant species (Fig. 1Bd), and its ¹⁷O NMR spectrum contained slightly upfield-shifted signals for free H₂O₂ ($\delta_{\text{O}} = 183.9$ ppm) and a bridging aqua ligand signal ($\delta_{\text{O}} = 51.3$ ppm; Fig. 1Cd). This conforms to ¹¹⁹Sn NMR being very sensitive to changes in both the first and second coordination sphere of Sn^{IV}, so the subtle changes in the general composition of Sn^{IV} complexes cause shifts of corresponding signals in ¹¹⁹Sn NMR spectra.

Subsequent addition of another half equivalent of H₂O resulted in the appearance of a high-field signal in ¹¹⁹Sn NMR ($\delta_{\text{Sn}} = -589.7$ ppm; Fig. 1Be) and a new high-field H₂O signal ($\delta_{\text{O}} = 31.9$ ppm) in the corresponding ¹⁷O NMR spectrum (Fig. 1Ce) that we assigned to complex SnCl₄(H₂O₂)(H₂O) (**2**; Fig. 1A). This substantial change in the chemical shift of the O atom of a coordinated H₂O suggested that it had changed from a bridging coordination mode to a terminal coordination mode. A gradual increase in the H₂O concentration (to a threefold molar excess of H₂O relative to SnCl₄) led to the appearance of new high-field signals in the ¹¹⁹Sn NMR spectra, indicating the complete substitution of H₂O₂ ligands in the coordination sphere of Sn^{IV} in the original complex to form [SnCl₄(H₂O)]₂(μ -H₂O) (**2'**; $\delta_{\text{Sn}} = -610.7$ ppm; Fig. 1Bf) and then the known¹⁵ SnCl₄ diaqua complex SnCl₄(H₂O)₂ (**3**; $\delta_{\text{Sn}} = -633.2$ ppm; Fig. 1Bg). The ¹⁷O NMR spectrum of this compound exhibited the signals of an aqua ligand and H₂O₂ at $\delta_{\text{O}} = 27.4$ and 181.7 ppm, respectively (Fig. 1Cf). The single resonance for the aqua ligand indicates a rapid exchange between the solvent and the ligand.

H₂O₂ ligands can also be substituted by other donor molecules. For example, the addition of a threefold molar excess (based on Sn) of MeOH to a SnCl₄-H₂O₂ system resulted in the formation of SnCl₄(MeOH)₂, as confirmed by ¹¹⁹Sn NMR ($\delta_{\text{Sn}} = -609.1$ ppm, Fig. 1Bh)¹⁶. Moreover, addition of MeCN to a solution of SnCl₄ in anhydrous H₂O₂ resulted in the immediate formation of a crystalline complex SnCl₄(MeCN)₂ (**4**, Supplementary Fig. 4), as confirmed by scXRD¹⁷. This ease with which H₂O₂ ligands can be substituted is consistent with the large difference between the PA of H₂O₂ (161.2 kcal mol⁻¹) and the PAs of H₂O, MeOH, and MeCN (165.2, 180.3, and 186.2 kcal mol⁻¹, respectively)⁸.

Synthesis and crystal structure of SnCl₄-H₂O₂ adducts with 18-crown-6

H₂O₂ always forms two hydrogen bonds, which stabilize crystalline adducts^{18,19}. Similarly, an H₂O₂ ligand in a complex with zinc(II) was previously found to form hydrogen bonds with the proton-accepting tosyl groups of neighboring ligands¹³. Additionally, the formation of crystalline adducts of octahedral SnCl₄(L)₂ complexes bearing small ligands (e.g., diaqua and MeOH) and large organic molecules such as cyclodextrins, cucurbiturils, cryptands, and crown ethers was previously demonstrated²⁰. In the current study, we examined whether SnCl₄-H₂O₂ systems can be stabilized by 18-crown-6 ether, because this compound is impervious to oxidation and contains six oxygen atoms, which can act as proton acceptors. Moreover, hydrogen bonding of H₂O₂ with 18-crown-6 ether was previously revealed by scXRD analysis of a corresponding peroxosolvate²¹.

Accordingly, crystals of **1-3** were obtained from solutions of SnCl₄ in 99.9 wt.% H₂O₂ in the presence of 18-crown-6 with and without H₂O,

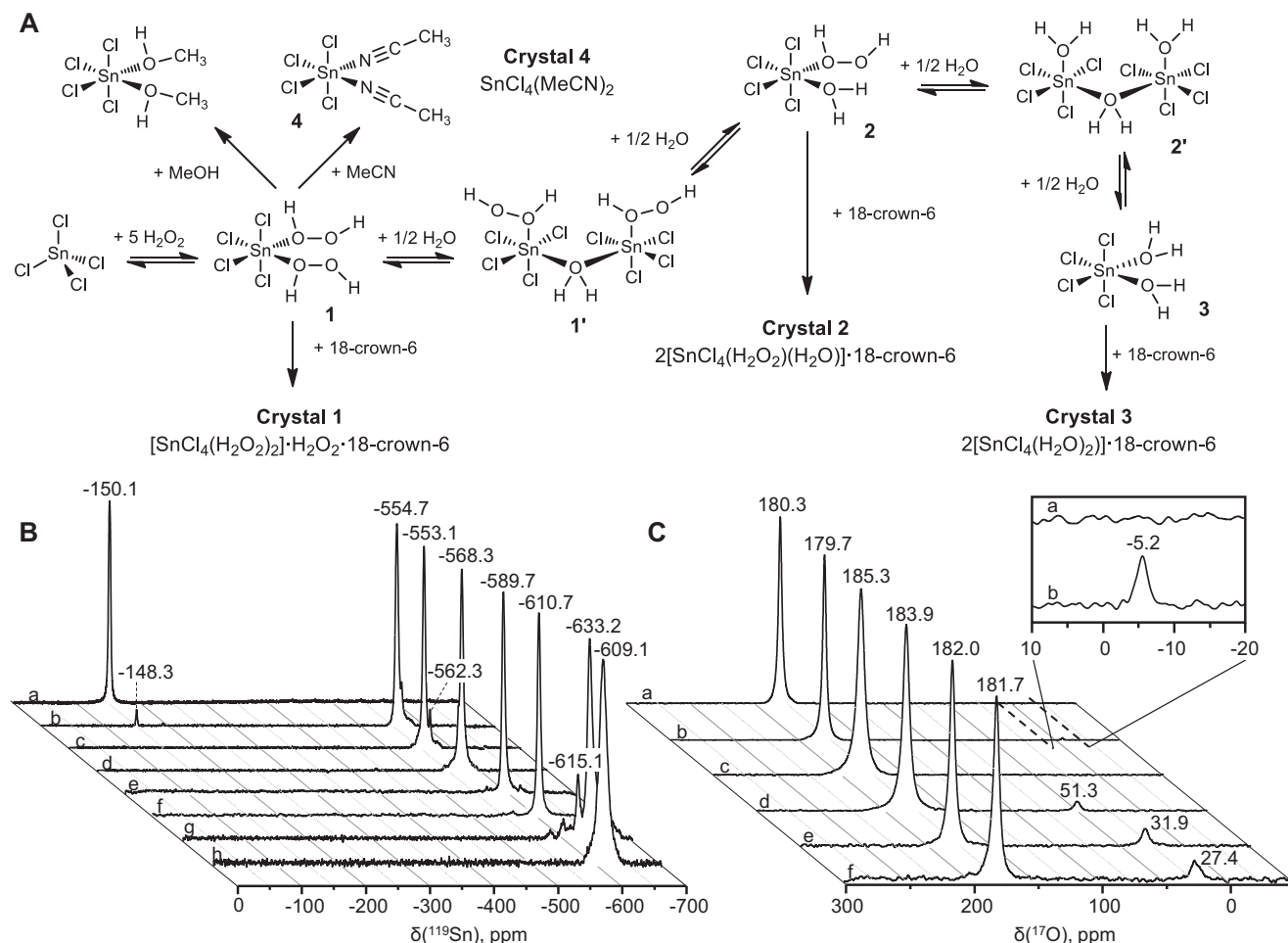


Fig. 1 | Complexation of tin tetrachloride in hydrogen peroxide solution supported by NMR spectroscopy. **A** Coordination of tin tetrachloride (SnCl_4) with hydrogen peroxide (H_2O_2), formation of crystalline compounds **1–4** and assumed intermediate complexes supported by ^{119}Sn and ^{17}O NMR. **B** ^{119}Sn nuclear magnetic resonance spectra of neat SnCl_4 (a); an $\text{SnCl}_4\text{--H}_2\text{O}_2$ (99.9%) system comprising a 1:5 molar ratio of SnCl_4 to H_2O_2 (b); 3M SnCl_4 in 99.9 wt.% H_2O_2 before (c) and after

addition of 0.5 moles (d), 1 mole (e), 1.5 moles (f), and 3 moles of H_2O with respect to Sn (g), and after addition of 3 moles of methanol with respect to Sn (h). **C** ^{17}O NMR spectra of 99.9 wt.% H_2O_2 before (a) and after addition of 1 wt.% of water (H_2O) (b); 3 M SnCl_4 in 99.9 wt.% H_2O_2 before (c) and after addition of 0.5 moles (d), 1 mole (e), and 3 moles of H_2O with respect to Sn (f).

respectively, and analyzed by scXRD (Supplementary Table 1). This confirmed that **1–3** consisted of complexes with the compositions suggested by the NMR studies and unveiled a rich set of non-covalent interactions (Fig. 2 and Supplementary Fig. 1). In **1–3**, the Sn^{IV} atom is present in a distorted octahedral environment with four chlorine atoms and two O atoms of H_2O_2 or H_2O molecules, resulting in a *cis* isomer with O–Sn–O angles significantly less than 90° (Fig. 2A,B, Supplementary Table 2). The distances between the Sn^{IV} and the O atoms of H_2O_2 (2.179(4) and 2.200(3) Å in **1**, and 2.225(3) Å in **2**) are much greater than those between the Sn^{IV} and the O atoms of H_2O (2.138(3) Å in **2**, and 2.133(2), 2.138(2) Å in **3**) (Table 1 and Supplementary Table 2). This reflects the weaker coordination of H_2O_2 to Sn^{IV} than of H_2O to Sn^{IV} , as confirmed by addition of H_2O resulting in the substitution of H_2O_2 by H_2O . Moreover, the Sn–O distances in the complexes with aqua ligands exhibit a narrow range, but those in the complexes with H_2O_2 ligands exhibit a broader range. This disparity suggests that Sn–O interactions in the latter complexes are more significantly influenced by the strength of second-sphere hydrogen bonding than those in the aqua complexes. Thus, this hydrogen bonding fine-tunes the coordination of the H_2O_2 ligands.

Interestingly, the H_2O_2 ligands in the structures of **1** and **2** do not form hydrogen bonds as proton acceptors. This is similar to the H_2O_2 hydrogen bonding in a previously reported¹³ Zn^{II} complex and may be

caused by coordination to the Lewis-acidic Sn species. Instead, the H_2O_2 and H_2O ligands participate as proton donors in hydrogen bonding with crown ether molecules (**1–3**), a chlorine atom in the adjacent SnCl_4 fragment (**2**), and solvate H_2O_2 (**1**) (Supplementary Tables 3–5). The O(3)···O(5) distance in **1** (2.542(5) Å) and the O(1)···O(6) distance in **2** (2.548(4) Å) between the Sn-bound peroxy-OH moiety and adjacent H_2O_2 and ether oxygen, respectively, are much shorter than those in crystalline 18-crown-6 peroxosolvate (2.761(1)–3.040(1) Å)²¹. Furthermore, to the best of our knowledge, these distances are shorter than previously reported O···O distances in hydrogen bonds formed by H_2O_2 in crystalline peroxosolvates²⁰. This suggests that the coordination of H_2O_2 with the Lewis acid (Sn^{IV}) in **1** and **2** results in an increase in the acidity of H_2O_2 that makes it form short hydrogen bonds. The phenomenon of hydrogen-bond enhancement due to coordination with Lewis acids has been observed in various hydrogen-bond donors^{22,23} and widely applied in catalysis^{24,25}. However, this phenomenon has not been reported to occur in complexes containing H_2O_2 .

Binding to Sn leads to a shortening of the O–O bond in coordinated H_2O_2 . Specifically, the O–O distances (1.422(5) and 1.443(5) Å in **1**, and 1.445(4) Å in **2**) are shorter than those in crystalline H_2O_2 (1.461(3) Å)²⁶ and cesium hexahydroperoxy stannate (1.482(2) Å)¹⁴. In addition, the two O–O fragments of the H_2O_2 ligands in **1** are almost

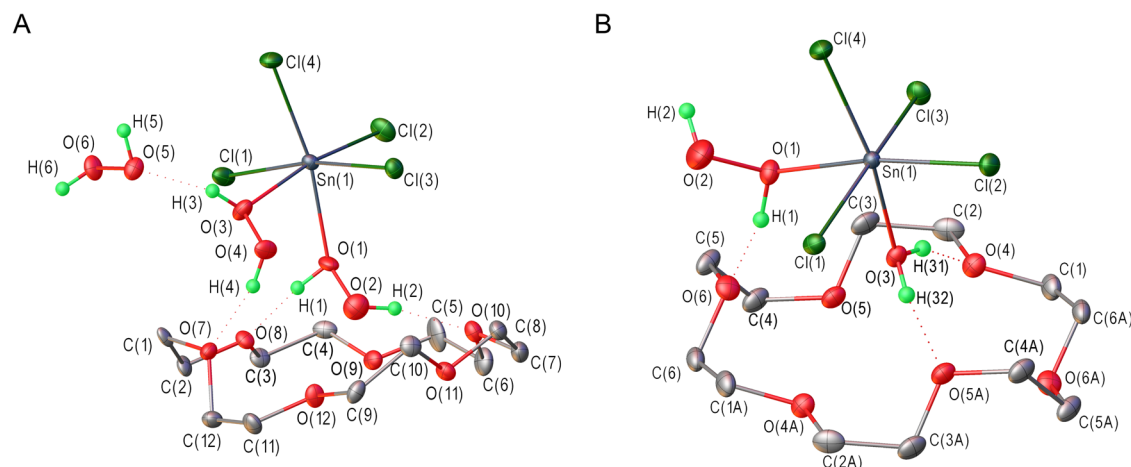


Fig. 2 | The crystal structures of hydrogen peroxide complexes with tin tetrachloride. A symmetric unit in **1**. **B** Asymmetric unit in **2**. 18-crown-6 molecule lies on crystallographic inversion center. Displacement ellipsoids are shown at a 50%

probability level. Hydrogen bonds are represented by dotted lines. The H atoms of the macrocyclic ether are omitted for clarity.

Table 1 | Selected geometric parameters obtained by scXRD analysis and DFT calculation (gas phase), and QTAIM-derived energetics for contacts involving the H₂O₂ ligand in 1 and 2 at the ω B97X-D3/TZVPP level of theory^a

Cpd	d(Sn–O ₂ H ₂), Å		$E_{\text{Sn–O}}$, ^b kcal mol ^{–1}	Contact	d(D...A), Å		d(H...A), Å		E_{intr}^b , kcal mol ^{–1}	ΣE_{intr} , kcal mol ^{–1}
	X-ray	DFT			X-ray	DFT	X-ray	DFT		
1	2.179(4)	2.261	16.4	O(1)H...O(8)	2.583(5)	2.642	1.74(3)	1.683	9.7	17.8
				O(2)H...O(10)	2.671(5)	2.733	1.82(3)	1.761	8.1	
	2.200(3)	2.323	13.4	O(3)H...O(5)	2.542(5)	2.690	1.74(3)	1.726	8.9	16.4
				O(4)H...O(7) ^c	2.730(5)	3.110	1.91(3)	2.419	2.0 ^d	
				O(4)H...O(12)	3.156(5)	2.837	2.60(4)	1.945	5.5	
2	2.225(3)	2.358	12.3	O(1)H...O(6)	2.548(4)	2.631	1.70(3)	1.704	9.4	13.4
				O(2)H...Cl(3) ^d	3.114(4)	3.142	2.33(4)	2.267	4.0	

^aSee Fig. 2 for atom labeling.

^bCalculated using Eq. 1 (see “Methods” section of the main text).

^cO(7) and O(12) were neighboring oxygen atoms, and peroxide O(4)H switched its position between these O atoms in the DFT calculations.

^dThe intramolecular O(2)–H...Cl(4) hydrogen bond was identified in the calculated structure.

parallel to each other (Supplementary Fig. 5). However, remarkably, there is no hydrogen bond between the H₂O₂ ligands, despite these neighboring molecules bearing acidic protons. Moreover, the interligand O...O distances in **1** (O(1)...O(3) = 2.844(5) Å and O(2)...O(4) = 3.019(6) Å) are shorter than the sum of their van der Waals radii (3.04 Å), which could indicate the presence of a weak contact (e.g., a chalcogen bond).

DFT calculations

To study the mutual influence of various types of bonding of H₂O₂ ligands we performed gas-phase DFT calculations for **1** and **2**. As mentioned above, the coordination of H₂O₂ with Sn^{IV} increases the acidity of H₂O₂, which increases the strength of the hydrogen bond that subsequently forms. According to DFT calculations, the sum of the energies of two hydrogen bonds formed by H₂O₂ molecules acting as proton donors correlates with the Sn–O distance, i.e., the high sum corresponds to the short distance, revealing the synergy between the coordination of an H₂O₂ ligand and its hydrogen bonding with the second coordination sphere (Table 1).

To highlight the synergy of primary (Sn–O) and secondary (hydrogen bond) interactions in an H₂O₂–Sn complex, we studied the interaction of an SnCl₄(H₂O₂)₂ complex with imidazole, which served as a model of proton-donating and proton-accepting molecules in the second coordination sphere. The imidazole moiety of histidine (His42)

plays an important role in the peroxidase catalytic cycle²⁷ contributing to the formation of the supposed iron-hydrogen peroxide complex with heme to give [Fe–OOH] form – a so-called Compound 0 – at the next step^{27,28}. DFT calculations were performed for SnCl₄(H₂O₂)₂, H₂O₂·C₃H₄N₂, SnCl₄(H₂O₂)₂·C₃H₄N₂, and analogs containing the imidazolium cation (C₃H₅N₂⁺), e.g., SnCl₄(H₂O₂)₂·C₃H₅N₂⁺ (Table 2, Supplementary Fig. 6). The optimized structure of the SnCl₄(H₂O₂)₂·C₃H₄N₂ adduct features the O–H...N hydrogen bond with an N...O distance of 2.622 Å, which correlates well with the corresponding interaction in the reported crystal structure of histidine peroxosolvate²⁹. Adduct SnCl₄(H₂O₂)₂·C₃H₅N₂⁺ contains an H₂O₂ ligand functioning as an acceptor of the acidic proton of the imidazolium cation, with an N...O distance of 2.967 Å.

In the SnCl₄(H₂O₂)₂·C₃H₄N₂ adduct, the hydrogen bonding of coordinated H₂O₂ with imidazole leads to the shortening of the Sn–O distance for the hydrogen-bonded H₂O₂ ligand. The N...O distance of the hydrogen bond of the H₂O₂ ligand is also shorter than that in imidazole peroxosolvate, H₂O₂·C₃H₄N₂. In contrast, the hydrogen bonding of peroxide oxygen with imidazolium in SnCl₄(H₂O₂)₂·C₃H₅N₂⁺ causes a substantial elongation of the corresponding Sn–O bond. This reflects the mutual influence of primary (Sn–O) and secondary (hydrogen) bonds that is further supported by the energy analysis. The value and sign of the cooperative effect, $\Delta\Delta H_{\text{coop}}$, for the SnCl₄(H₂O₂)₂ adduct with a second-coordination-sphere proton acceptor (imidazole molecule) or

Table 2 | Bond distances (d, in Å) and energies (in kcal mol⁻¹) for the hydrogen and coordination bonds in SnCl₄(H₂O)₂, H₂O₂·C₃H₄N₂, SnCl₄(H₂O)₂·C₃H₄N₂, H₂O₂·C₃H₅N₂⁺, and SnCl₄(H₂O)₂·C₃H₅N₂⁺ at the ωB97X-D3/TZVPP level of theory

SnCl ₄ (H ₂ O) ₂			H ₂ O ₂ ·C ₃ H ₄ N ₂			SnCl ₄ (H ₂ O) ₂ ·C ₃ H ₄ N ₂		
ΔH_f^a	-8.99 (-4.12*)	-6.36	-19.88 (-15.01*)					
Contact	d	E_{int}^b	d	E_{int}	d	E_{int}	$\Delta\Delta H_{coop}^c$	
Sn-O1	2.371	11.7	-	-	2.284	15.1	-3.06	
Sn-O3	2.334	13.1	-	-	2.339	12.9		
N...(H)O2	-	-	1.742	8.3	1.608	10.9		
			H ₂ O ₂ ·C ₃ H ₅ N ₂ ⁺			SnCl ₄ (H ₂ O) ₂ ·C ₃ H ₅ N ₂ ⁺		
ΔH_f	-2.54	-11.52 (-6.66*)						
Contact	d	E_{int}^b	d	E_{int}	d	E_{int}	$\Delta\Delta H_{coop}$	
Sn-O1	-	-	-	-	2.432	9.9	1.06	
Sn-O3	-	-	-	-	2.337	13.0		
N(H)...O2	1.837	7.0	1.988	4.9				

*Energy relative to SnCl₄(H₂O)₂.

^aFormation enthalpies, ΔH_f , calculated relative to isolated reactants.

^bBond energies, E_{int} , calculated using Eq. 1 (see "Methods" section of the main text).

^c $\Delta\Delta H_{coop}$, calculated using Eq. 2 (see "Methods" section of the main text).

Table 3 | Distances between each Sn^{IV} coordination center and its ligand's hydrogen-bond acceptor

Compound	Method	d(Sn...A) (A = O, Cl, or N), Å		
		H ₂ O ₂		H ₂ O
		Proximal	Distal	
[SnCl ₄ (H ₂ O ₂) ₂]:H ₂ O ₂ :18-crown-6 (1)	scXRD	4.217 (O) 4.274 (O)	4.867 (O) 4.548 (O)	–
2[SnCl ₄ (H ₂ O ₂)(H ₂ O)]:18-crown-6 (2)	scXRD	4.281 (O)	5.315 (Cl)	4.031 (O) 4.339 (O)
2[SnCl ₄ (H ₂ O ₂) ₂]:18-crown-6 (3)	scXRD	–	–	4.011 (O) 4.415 (O) 4.187 (O) 4.664 (Cl)
SnCl ₄ (H ₂ O ₂) ₂ :C ₃ H ₄ N ₂	DFT	–	4.695 (N)	–

proton donor (imidazolium cation) estimated by Eq. 2 was used as a measure of the synergism or antagonism of primary and secondary interactions³⁰.

A preliminary attempt to protonate SnCl₄(H₂O₂)₂ in gas-phase DFT calculations led to the dissociation of this complex. Therefore, we expected that the interaction of a proton donor with an H₂O₂ ligand would lead to a decrease in the stability of the complex. Indeed, hydrogen bonding of imidazolium to a distal oxygen has an antagonistic energetic effect ($\Delta\Delta H_{\text{coop}} = 1.06 \text{ kcal mol}^{-1}$). In contrast, a synergistic effect was found between H₂O₂ coordination and its proton donation to the imidazole fragment ($\Delta\Delta H_{\text{coop}} = -3.06 \text{ kcal mol}^{-1}$).

The distances between the Sn^{IV} coordination center and the ligand hydrogen-bond acceptor in the scXRD data of **1–3** and the calculated adduct SnCl₄(H₂O₂)₂:C₃H₄N₂ are presented in Table 3. As expected, the distances between Sn^{IV} and the hydrogen-bond acceptor of the aqua ligand correlate with those for the proximal hydroxo group of the H₂O₂ ligand. However, the distance between the coordination center and the acceptor of the distal hydroxo group of the H₂O₂ ligand is always longer than that for the aqua ligand when the acceptor is of the same type. This observation also calls for a speculation on the coordination of H₂O₂ to enzymes' heme, which occurs in aqueous systems. The Fe...N^{His42} distance in peroxidases is approximately 5.7 Å^{31,32}, which is too long for activation of H₂O but is suitable for activation of H₂O₂. In this hydrophobic pocket, the OH...N hydrogen bonding of the distal OH group to His42 should stabilize the binding of H₂O₂ to a heme Fe. One can speculate that due to this unique hydrogen bond of the distal proton, the enzyme can differentiate between Fe·OH₂ and Fe·O₂H₂ complexes, as the cooperative effect (as estimated herein; Table 2) would overcome a stronger Fe–O bond with H₂O than with H₂O₂ and stabilize the encounter [Fe–O₂H₂] complex. Furthermore, as the coordination to an Fe ion increases the acidity of the proximal OH group, it should facilitate deprotonation of Compound 0 yielding [Fe–OOH] hydroperoxo complex.

The scarcity of structurally resolved H₂O₂ complexes has hindered an examination of the structure and bonding of H₂O₂ ligands in reaction intermediates and life-sustaining biocomplexes. This limitation is attributable to H₂O₂ being less basic than the common coordinating solvents by which it is replaced in a metal coordination sphere. In addition, H₂O₂ is poorly soluble in most non-coordinating solvents. In this study, we suggested a synthetic approach based on the use of pure H₂O₂ as both solvent and ligand. Thus, coordinatively unsaturated SnCl₄ effectively binds H₂O₂ yielding SnCl₄(H₂O₂)₂, which was characterized by ¹¹⁹Sn and ¹⁷O NMR spectroscopy. This complex comprises rather strong Sn–O bonds (12–16 kcal mol⁻¹ according to DFT analysis), but its H₂O₂ ligands could be easily substituted in the Sn^{IV} coordination sphere by molecules of higher basicity, i.e., MeOH, MeCN, and even H₂O. The use of 18-crown-6 as a bulky yet stable H₂O₂-proton acceptor stabilized SnCl₄(H₂O₂)₂ as its 18-crown-6 adduct (**1**). The addition of H₂O gave the stepwise substitution products **2** and **3**.

ScXRD analysis of these complexes revealed their rich set of non-covalent interactions, including the shortest O(H)···O distances in hydrogen bonds formed by H₂O₂ in known crystal structures. Complemented by the results of our DFT analysis, this demonstrates the synergistic effects of a coordination bond with Sn^{IV} and hydrogen bonding with a second coordination sphere on the properties of an H₂O₂ ligand. The energies of two hydrogen bonds formed by each H₂O₂ ligand acting as a proton donor correlate with the Sn–O distance in **1** and **2**, with the higher hydrogen-bond energy value corresponding to the shorter Sn–O distance. Remarkably, none of the H₂O₂ ligands participated in hydrogen bonding as proton acceptors, despite the proximity of acidic protons. Our DFT study of model SnCl₄(H₂O₂)₂ adducts with imidazole/imidazolium suggested that this is due to the antagonistic energetic effect of such interactions.

In summary, this study demonstrated that second-coordination-sphere hydrogen bonding plays a key role in the stabilization of H₂O₂ coordination. The non-covalent interactions of H₂O₂ ligands not only contribute to the total energy of the system but also increase the basicity of the H₂O₂ ligand, which enhances coordination bonding. This explains why H₂O₂ coordination, despite being impossible in aqueous solution under equilibrium conditions, is common in nature, such as in oxygenases. Coordination with a Lewis acid has previously been proposed to be a key factor in the activation of H₂O₂ for the oxidation of organic substrates⁵. Therefore, we envisage prospects for the development of new catalytic systems in which the distance between the coordination center and the hydrogen bond acceptor is approximately 5 Å. This would make it possible to utilize the synergism of the primary and secondary interactions and ensure the coordination of H₂O₂ in the presence of H₂O or other polar molecules.

Methods

Synthesis of anhydrous H₂O₂ and SnCl₄

Caution! Working with concentrated H₂O₂ and chlorine is hazardous and requires appropriate precautions to be taken.

Small amounts of anhydrous H₂O₂ can be obtained from its crystalline adducts with organic compounds^{33,34}. However, this requires the use of organic solvents (diethyl ether or MeCN) that may absorb H₂O and other impurities, and also may remain in the product H₂O₂ and thus interact with SnCl₄ in the next step. Therefore, in the current study, we purified commercial H₂O₂ via a two-stage vacuum distillation process. First, 30 wt.% H₂O₂ was distilled under vacuum to remove stabilizers and other impurities and afford 18 wt.% pure aqueous H₂O₂. Second, this H₂O₂ solution was concentrated by rectification under vacuum, controlling the boiling by passing argon (Ar), to afford 99.9 wt.% H₂O₂ (as determined by permanganometry; Supplementary Methods).

As commercial SnCl₄ may contain impurities that can catalyze H₂O₂ decomposition, we synthesized SnCl₄ from ultrapure metal Sn by chlorination followed by rectification (Supplementary Methods).

NMR spectroscopy

The solutions for NMR experiments were prepared in an Ar-filled glovebox (O₂ and H₂O concentrations < 0.1 ppm) and then immediately placed in the spectrometer (Supplementary Methods). The time between the preparation of the solutions and the NMR experiments did not exceed 10 min. ¹⁷O and ¹¹⁹Sn NMR spectra (δ , ppm) were collected at 303 K on a Bruker AVANCE III 600 spectrometer operating at 81.36 MHz and 223.79 MHz, respectively. ¹⁷O and ¹¹⁹Sn chemical shifts were referenced to H₂O and tetramethyltin, respectively. NMR spectra were processed using TopSpin software.

ScXRD

Single crystals of **1–4** that were suitable for X-ray analysis were collected from the corresponding mother liquors without additional recrystallization, placed on microscope slides, and then coated with a

perfluorinated oil (Fomblin YR-1800). Subsequently, appropriate single crystals were mounted on MicroMeshes™ (MiTeGen) and then immediately positioned beneath a cold stream of nitrogen on the diffractometer, which was a Bruker D8 Venture instrument that used graphite monochromatized molybdenum K-alpha radiation ($\lambda = 0.71073 \text{ \AA}$) and was operated in ω -scan mode at 100 K. Absorption corrections based on measurements of equivalent reflections were applied³⁵. The structures were solved by direct methods and refined by full matrix least-squares on F^2 with anisotropic thermal parameters for all non-hydrogen atoms³⁶. The hydrogen atoms of H_2O_2 and H_2O molecules in **1–3** were found from difference Fourier synthesis and refined with distance restraints. The hydrogen atoms of 18-crown-6 in **1–3** and MeCN solvent in **4** were placed in idealized positions and refined using a riding model. Additional crystallographic data for **1–4** are provided in the Supplementary Information (Supplementary Figs. 1–4, Supplementary Tables 1–5).

ScXRD of **1** indicated a relatively short distance between H(4) and O(12), i.e., 2.60(4) Å. However, it was much longer than a typical O–H...O hydrogen bond, and its O–H...O angle (124.7°) lay outside the normal range. Thus, this contact was not attributable to a hydrogen bond and appeared to be a forced contact due to crystal packing.

The X-ray structure of **4** exhibited better resolution (see Supplementary Table 1) than that of a previously reported structure¹⁷.

DFT calculations

Clusters containing the fragments of asymmetric units of **1** and **2** were taken from the corresponding scXRD data, and calculations were performed using various approaches (Supplementary Methods, Supplementary Data 1). Optimization at the $\omega\text{B97X-D3/TZVPP}$ level of theory afforded the best correlation between the calculated Sn–O distances and those obtained from scXRD (Table 1) and is therefore used in the discussion of the results below. The quantum theory of atoms in molecules was applied to analyze the electron density parameters at the O–H...O hydrogen-bond critical points (Table 1 and Supplementary Table 6).

In these calculations, H_2O was used as a solvent (in the conductor-like polarizable continuum model approach) because it closely approximates the solvent properties of H_2O_2 (i.e., its dielectric constant and acidity/basicity) and because polar solvents typically weaken non-covalent interactions, meaning that the detection of a pronounced effect in such a solvent serves as strong evidence of the proposed concept.

The energies of non-covalent interactions in the optimized clusters of **1** and **2** were estimated according to Espinosa's approach³⁷ (Eq. 1) and are presented in Table 1.

$$E_{\text{int}}[\text{kcal mol}^{-1}] = 269.2G_b[\text{atomic units}] \quad (1)$$

where G_b is a Lagrangian of kinetic energy density at the bond critical point.

The cooperative effect, $\Delta\Delta H_{\text{coop}}$, was calculated according to ref. 30:

$$\Delta\Delta H_{\text{coop}}(\text{ABC}) = H_{\text{ABC}} - (H_{\text{AB}} + H_{\text{BC}} + H_{\text{AC}}) + (H_{\text{A}} + H_{\text{B}} + H_{\text{C}}) \quad (2)$$

where H are enthalpies of the corresponding trimer ($\text{SnCl}_4(\text{H}_2\text{O}_2)_2 \cdot \text{C}_3\text{H}_{4+n}\text{N}_2^{n+}$), dimers ($\text{SnCl}_4(\text{H}_2\text{O}_2)_2$, $\text{H}_2\text{O}_2 \cdot \text{C}_3\text{H}_{4+n}\text{N}_2^{n+}$ and $\text{SnCl}_4(\text{H}_2\text{O}_2) // \text{C}_3\text{H}_{4+n}\text{N}_2^{n+}$) and monomers ($\text{SnCl}_4(\text{H}_2\text{O}_2)$, H_2O_2 and $\text{C}_3\text{H}_{4+n}\text{N}_2^{n+}$) at the trimer geometry; $n = 0$ for imidazole, and $n = 1$ for imidazolium.

Data availability

The X-Ray crystallographic data for the structures reported in this Article have been deposited at the Cambridge Crystallographic Data Centre (CCDC) under deposition numbers CCDC 2260843 (**1**),

2260844 (**2**), 2260845 (**3**) and 2260846 (**4**). These data can be obtained free of charge via <https://www.ccdc.cam.ac.uk/structures/>. The equilibrium Cartesian coordinates data generated in this study are provided as the Supplementary Data 1. All data are available in the main text, the Supplementary Information and from the corresponding authors.

References

1. Glasauer, A. & Chandel, N. S. ROS. *Curr. Biol.* **23**, R100–R102 (2013).
2. Dickinson, B. C. & Chang, C. J. Chemistry and biology of reactive oxygen species in signaling or stress responses. *Nat. Chem. Biol.* **7**, 504–511 (2011).
3. D'Autréaux, B. & Toledano, M. B. ROS as signaling molecules: mechanisms that generate specificity in ROS homeostasis. *Nat. Rev. Mol. Cell Biol.* **8**, 813–824 (2007).
4. Rhee, S. G. H_2O_2 , a Necessary evil for cell signaling. *Science* **312**, 1882–1883 (2006).
5. Ma, Z. et al. Peroxides in metal complex catalysis. *Coord. Chem. Rev.* **437**, 213859 (2021).
6. Novikov, A. S., Kuznetsov, M. L., Rocha, B. G. M., Pombeiro, A. J. L. & Shul'pin, G. B. Oxidation of olefins with H_2O_2 catalysed by salts of group III metals (Ga, In, Sc, Y and La): epoxidation versus hydroperoxidation. *Catal. Sci. Technol.* **6**, 1343–1356 (2016).
7. Costa, G. J. & Liang, R. Understanding the multifaceted mechanism of compound I formation in unspecific peroxxygenases through multiscale simulations. *J. Phys. Chem. B* **127**, 8809–8824 (2023).
8. Hunter, E. P. L. & Lias, S. G. Evaluated gas phase basicities and proton affinities of molecules: an update. *J. Phys. Chem. Ref. Data* **27**, 413–656 (1998).
9. Mirza, S. A., Bocquet, B., Robyr, C., Thomi, S. & Williams, A. F. Reactivity of the coordinated hydroperoxo ligand. *Inorg. Chem.* **35**, 1332–1337 (1996).
10. DiPasquale, A. G. & Mayer, J. M. Hydrogen peroxide: A poor ligand to gallium tetraphenylporphyrin. *J. Am. Chem. Soc.* **130**, 1812–1813 (2008).
11. Wallen, C. M., Palatinus, L., Bacsa, J. & Scarborough, C. C. Hydrogen peroxide coordination to cobalt(II) facilitated by second-sphere hydrogen bonding. *Angew. Chem. Int. Ed.* **55**, 11902–11906 (2016).
12. Wallen, C. M., Bacsa, J. & Scarborough, C. C. Coordination of hydrogen peroxide with late-transition-metal sulfonamido complexes. *Inorg. Chem.* **57**, 4841–4848 (2018).
13. Wallen, C. M., Bacsa, J. & Scarborough, C. C. Hydrogen peroxide complex of zinc. *J. Am. Chem. Soc.* **137**, 14606–14609 (2015).
14. Churakov, A. V. et al. Cesium hydroperoxostannate: first complete structural characterization of a homoleptic hydroperoxocomplex. *Inorg. Chem.* **49**, 4762–4764 (2010).
15. Xi-an, M., Xiao-zeng, Y. & An-bang, D. ^{119}Sn NMR spectra of $\text{SnCl}_4 \cdot 5\text{H}_2\text{O}$ in $\text{H}_2\text{O}/\text{HCl}$ solutions. *Inorg. Chim. Acta* **156**, 177–178 (1989).
16. Blunden, S. J., Cusack, P. A., Smith, P. J. & Barnard, P. W. C. Studies on the interaction of inorganic tin compounds with methyl 4,6-O-benzylidene- α -D-glucopyranoside and related molecules. *Inorg. Chim. Acta* **72**, 217–222 (1983).
17. Webster, M. & Blayden, H. E. Crystal structure and vibrational spectrum of tetrachlorotin(IV)-bisacetone nitrile. *J. Chem. Soc. A* **2443**, 2451 (1969).
18. Chernyshov, I. Y. et al. Peroxosolvates: Formation criteria, H_2O_2 hydrogen bonding, and isomorphism with the corresponding hydrates. *Cryst. Growth Des.* **17**, 214–220 (2017).
19. Grishanov, D. A. et al. Hydrogen peroxide insular dodecameric and pentameric clusters in peroxosolvate structures. *Angew. Chemie Int. Ed.* **56**, 15241–15245 (2017).
20. Groom, C. R., Bruno, I. J., Lightfoot, M. P. & Ward, S. C. The Cambridge structural database. *Acta Crystallogr.* **B72**, 171–179 (2016).
21. Medvedev, A. G. et al. Fast quantum approach for evaluating the energy of non-covalent interactions in molecular crystals: the case

- study of intermolecular h-bonds in crystalline peroxosolvates. *Molecules* **27**, 4082 (2022).
22. Chin, J., Chung, S. & Kim, D. H. Synergistic effect between metal coordination and hydrogen bonding in phosphate and halide recognition. *J. Am. Chem. Soc.* **124**, 10948–10949 (2002).
 23. Nickerson, D. M., Angeles, V. V., Auvil, T. J., So, S. S. & Mattson, A. E. Internal lewis acid assisted ureas: tunable hydrogen bond donor catalysts. *Chem. Commun.* **49**, 4289–4291 (2013).
 24. Gong, L., Chen, L.-A. & Meggers, E. Asymmetric catalysis mediated by the ligand sphere of octahedral chiral-at-metal complexes. *Angew. Chem. Int. Ed.* **53**, 10868–10874 (2014).
 25. Larionov, V. A., Feringa, B. L. & Belokon, Y. N. Enantioselective “organocatalysis in disguise” by the ligand sphere of chiral metal-templated complexes. *Chem. Soc. Rev.* **50**, 9715–9740 (2021).
 26. Savariault, J. M. & Lehmann, M. S. Experimental determination of the deformation electron density in hydrogen peroxide by combination of X-ray and neutron diffraction measurements. *J. Am. Chem. Soc.* **102**, 1298–1303 (1980).
 27. Poulos, T. L. Heme enzyme structure and function. *Chem. Rev.* **114**, 3919–3962 (2014).
 28. Sengupta, K., Chatterjee, S. & Dey, A. Catalytic H₂O₂ disproportionation and electrocatalytic O₂ reduction by a functional mimic of heme catalase: direct observation of Compound O and Compound I in situ. *ACS Catal.* **6**, 1382–1388 (2016).
 29. Oya, Y., Takenaka, A., Ochi, T. & Yamamoto, K. The biological activity of hydrogen peroxide V. The crystal structure of a histidine-peroxide adduct and its biological activities. *Mutat. Res. Mol. Mech. Mutagen.* **266**, 281–289 (1992).
 30. Tebben, L., Mück-Lichtenfeld, C., Fernández, G., Grimme, S. & Studer, A. From additivity to cooperativity in chemistry: can cooperativity be measured? *Chem. – Eur. J.* **23**, 5864–5873 (2017).
 31. Derat, E. & Shaik, S. The Poulos–Kraut mechanism of Compound I formation in horseradish peroxidase: a QM/MM study. *J. Phys. Chem. B* **110**, 10526–10533 (2006).
 32. Berglund, G. I. et al. The catalytic pathway of horseradish peroxidase at high resolution. *Nature* **417**, 463–468 (2002).
 33. Cooper, M. S., Heaney, H., Newbold, A. J. & Sanderson, W. R. Oxidation reactions using urea-hydrogen peroxide; a safe alternative to anhydrous hydrogen peroxide. *Synlett* **1990**, 533–535 (1990).
 34. Cookson, P. G., Davies, A. G. & Fazal, N. The 1,4-diazaf[2.2.2] bicyclocloctane–hydrogen peroxide complex as a source of anhydrous hydrogen peroxide: the preparation of bis(trialkylsilyl) peroxides. *J. Organomet. Chem.* **99**, C31–C32 (1975).
 35. SADABS. Bruker/Siemens Area Detector Absorption Correction Program, v. 2016/2, (Bruker AXS Inc., Madison, Wisconsin, USA, 2016).
 36. Sheldrick, G. M. Crystal structure refinement with SHELXL. *Acta Crystallogr.* **C71**, 3–8 (2015).
 37. Mata, I., Alkorta, I., Espinosa, E. & Molins, E. Relationships between interaction energy, intermolecular distance and electron density properties in hydrogen bonded complexes under external electric fields. *Chem. Phys. Lett.* **507**, 185–189 (2011).

Acknowledgements

This work was supported by the Russian Science Foundation (grant no. 22-13-00426, <https://rscf.ru/en/project/22-13-00426/>). A.A.K. and M.V.B. acknowledge the support from the City University of Hong Kong (Project 7006013). O.L. acknowledges the Israel Science Foundation

(grant number 1215/19) for financial support. The X-ray diffraction studies were performed using the equipment of the JRC PMR IGIC RAS. The NMR studies were performed using the equipment of the CKP FMI IPCE RAS. A.G.M. and P.V.P. acknowledge Dr. A.V. Churakov for helpful discussion.

Author contributions

P.V.P. conceived the project; the project was supervised by P.V.P., O.L. and M.V.B.; P.V.P., M.V.B. and O.L. gathered the fundings and contributed equally. Conceptualization of the synthesis and NMR spectra assignment was provided by P.V.P.; A.A.M. and P.A.E. prepared the hydrogen peroxide; A.G.M. and P.A.E. prepared the solutions for NMR studies and performed synthesis of the crystals; A.G.M. conducted scXRD experiment and described the crystal structures; E.S.B., G.A.K. and Yu.G.G. performed the NMR studies; O.A.F., N.V.B. and E.S.S. conducted DFT calculations and provided discussion of the DFT results; M.N.B. performed SnCl₄ synthesis and purification; A.A.K. analyzed the literature on the hydrogen peroxide complexes; All authors discussed the results; P.V.P., M.V.B., and O.L. wrote the paper with input from all of the authors.

Competing interests

The authors declare no competing interests.

Additional information

Supplementary information The online version contains supplementary material available at <https://doi.org/10.1038/s41467-024-50164-9>.

Correspondence and requests for materials should be addressed to Maria V. Babak, Ovadia Lev or Petr V. Prikhodchenko.

Peer review information *Nature Communications* thanks Ruibin Liang, Christian Wallen and the other, anonymous, reviewer(s) for their contribution to the peer review of this work. A peer review file is available.

Reprints and permissions information is available at <http://www.nature.com/reprints>

Publisher's note Springer Nature remains neutral with regard to jurisdictional claims in published maps and institutional affiliations.

Open Access This article is licensed under a Creative Commons Attribution 4.0 International License, which permits use, sharing, adaptation, distribution and reproduction in any medium or format, as long as you give appropriate credit to the original author(s) and the source, provide a link to the Creative Commons licence, and indicate if changes were made. The images or other third party material in this article are included in the article's Creative Commons licence, unless indicated otherwise in a credit line to the material. If material is not included in the article's Creative Commons licence and your intended use is not permitted by statutory regulation or exceeds the permitted use, you will need to obtain permission directly from the copyright holder. To view a copy of this licence, visit <http://creativecommons.org/licenses/by/4.0/>.

© Crown 2024